Molecular Crystals and Liquid Crystals Science and Technology. Section A. Molecular Crystals and Liquid Crystals

Publication details, including instructions for authors and subscription information:
http://www.tandfonline.com/loi/gmcl19

COMPUTER SIMULATION OF THE HOMEOTROPIC TO FOCAL CONIC TRANSITION IN CHOLESTERICS

James E. Anderson [a] , Philip Watson [a] , Tod Ernst [b] & Philip J. Bos [a]

[a] Chemical Physics Interdisciplinary Program, Kent State University, Kent, Ohio, 44242, USA

[b] Liquid Crystal Institute, Kent State University, Kent, Ohio, 44242, USA

Version of record first published: 24 Sep 2006

To cite this article: James E. Anderson, Philip Watson, Tod Ernst & Philip J. Bos (2001): COMPUTER SIMULATION OF THE HOMEOTROPIC TO FOCAL CONIC TRANSITION IN CHOLESTERICS, Molecular Crystals and Liquid Crystals Science and Technology. Section A. Molecular Crystals and Liquid Crystals, 366:1, 909-918

To link to this article: http://dx.doi.org/10.1080/10587250108024034

Mol. Cryst. and Liq. Cryst., 2001, Vol. 366, pp. 909-918
Reprints available directly from the publisher
Photocopying permitted by license only

Computer Simulation of the Homeotropic to Focal Conic Transition in Cholesterics

JAMES E. ANDERSON[a], PHILIP WATSON[a], TOD ERNST[b] and PHILIP J. BOS[a]

[a]*Chemical Physics Interdisciplinary Program and* [b]*Liquid Crystal Institute, Kent State University, Kent, Ohio 44242, USA*

Previous reports have proposed mechanisms for the homeotropic to focal conic transition in cholesterics. In this report, we present quantitative numerical modeling of this transition. We will show that the simulation shows the existence of the transient planar state, agreeing with previous experimental findings. We will also demonstrate that the simulations never show energy densities high enough to form isotropic regions, demonstrating that this transition is a continuous process. Instead of introducing isotropic regions, the system transforms through an undulation distortion which strongly resembles a Helfrich-Hurault distortion. This simulation is compared with two experimental samples: one with parallel boundary conditions and one with perpendicular boundary conditions. The simulations are compared with dynamical capacitive measurements and microscope photographs, and found to agree very well. We will present detailed drawings of the director configuration during this transition. The agreement of this simulation with the experimental data shows that the mechanism of this transition is now well understood.

INTRODUCTION

In the cholesteric liquid crystal phase, the liquid crystal director (the average orientation of the long axis of the molecule) rotates in space about some axis [1]. The distance for the director to spatially twist 360 degrees is defined as the pitch, P. The unstrained (intrinsic) pitch is called P_0, with wavenumber q_0 ($= 2\pi/P_0$). This periodicity causes Bragg reflection of light with peak wavelength $\lambda_{max} = \langle n \rangle \times P_0$, and of spectral width $\Delta\lambda = \Delta n \times P_0$ [1]. Here $\langle n \rangle$ is the average index of refraction, and Δn is the birefringence of the material.

The director of a nematic can be made to rotate if a chiral dopant (a material that lacks mirror symmetry) is introduced into the system [2].

In the confined geometry of a liquid crystal cell, cholesteric material can exist in a number of textural states. If the helical axes are pointing approximately perpendicular to the substrates and the pitch is unstrained, the system is in the planar (**P**) state. The homeotropic (**H**) state is characterized by the directors being approximately aligned with one another as in a nematic, and pointing perpendicular to the substrates [1]. For cells having $d/P_0 > K_{33}/2K_{22}$ (typically ≈ 1), the **H** state can only be achieved by applying a sufficiently large external field [3]. Since it is the most common method, an electric field was used in this study to induce this state. To achieve the transition from a twisted structure to the **H** state, the field must be above the critical value, E_{CN}, given in equation (1) [1]. Greubel et al. derived the field below which the system will drop from the **H** state to a twisted state, assuming homeotropic boundary conditions, which is given in equation (2) [3].

$$E_{CN} = \left(\frac{\pi^2}{P_0}\right)\sqrt{\frac{K_{22}}{\varepsilon_0 \Delta\varepsilon}} \qquad (1) \qquad E_{NC} = \left(\frac{\pi}{P_0}\right)\sqrt{\frac{4K_{22}^2 - \left(\frac{P_0 K_{33}}{d}\right)^2}{\varepsilon_0 \Delta\varepsilon K_{33}}} \qquad (2)$$

In the focal conic (**FC**) state, the directors again exhibit an intrinsic twist about some axis, with the axis approximately parallel to the substrates [1]. If the system is in the **H** state, and the field is reduced to a value of roughly E_{NC} the system will transform from the **H** state to the **FC** state [3,4]. Yang et al. gave experimental results suggesting the existence of the transient planar (**TP**) state in the transition from the **H** state to the **FC** state at some voltages [4]. The **TP** state is similar to the **P** state, with the exception that the system has a longer pitch ($P^* \sim P_0 \times K_{33}/K_{22}$) [4]. It does not at first appear physically intuitive for the system to pass through the **TP** state during this transition. It would seem easier for the system to go directly to the **FC** state. In this paper, we show that quantitative numerical simulation indeed shows the system passing through the **TP** state.

It has also been assumed that the transition from the **H** state to the **FC** state required the introduction of isotropic regions. This is due to the fact that, under a microscope, many domain regions are seen. We will investigate this here and show that the introduction of such regions are energetically unfavorable.

NUMERICAL SIMULATIONS

The method used to calculate the director structure of the liquid crystal system is based on the fact that nature acts to minimize the free energy. The expression for the free energy density of a liquid crystal system in terms of the director, ***n***, is given by equation (3) [1].

$$f_g = \frac{1}{2}K_{11}(\nabla \bullet \hat{n})^2 + \frac{1}{2}K_{22}(\hat{n} \bullet \nabla \times \hat{n} + q_0)^2 + \frac{1}{2}K_{33}|(\hat{n} \times \nabla \times \hat{n})|^2 - \frac{1}{2}\vec{D} \bullet \vec{E} \quad (3)$$

Here, K_{11}, K_{22}, and K_{33} are the elastic constants for splay, twist and bend, respectively, $\boldsymbol{D}$ is the electric displacement and $\boldsymbol{E}$ is the electric field.

During the initial stages of the transition from the **H** state to the **FC** state, the experimental data as shown below suggests a 1-dimensional transition. However, because we desired information on the latter part of the transition, we allowed the system to vary over 2 spatial dimensions.

It has been found that writing this free energy as a function of the order parameter tensor, $\boldsymbol{Q}$, instead of the director, $\boldsymbol{n}$, when calculating director configurations can cause non-physical results [5]. Therefore, the vector approach was employed here.

Ignoring flow of the director, the dynamics of the director reorientation can be calculated by setting the functional derivatives of the free energy density with respect to each director component (the elastic torque) equal to the rotational torque on that component as shown in equation (4) [6].

$$\gamma_1 \frac{dn_i}{dt} = -\left[f_g\right]_{n_i} + \lambda n_i \;, i = x,y,z \quad (4) \qquad \left[f_g\right]_{n_i} = \frac{\partial f}{\partial n_i} - \frac{d}{dx}\left(\frac{\partial f}{\partial \frac{dn_i}{dx}}\right) - \frac{d}{dz}\left(\frac{\partial f}{\partial \frac{dn_i}{dz}}\right) \quad (5)$$

Where γ_1 is the rotational viscosity.

In equation (4), the Lagrange multiplier, λ, is used to maintain the unit length of the director. However, we cannot solve this equation for both the Lagrange multiplier and a numerical update formula for n_i. Therefore, the λ term is dropped and $\boldsymbol{n}$ is renormalized to have unit length after each time step [7,8].

Because the dielectric constant is anisotropic, the electric potential at each point depends on the director orientation at that and surrounding points. When Gauss's Law is discretized, an equation linear in these values results [8]. This linear equation can then be solved to yield a numerical update equation for the potential at the current grid point in terms of the neighboring values of potential and director components.

We found the calculation to be in a metastable equilibrium when homeotropic boundary conditions were used and the initial director configuration was exactly $\boldsymbol{n}$ = (0,0,1) everywhere. To avoid this, we started both calculations with some amount of random noise. The initial director configurations were calculated by first setting n_x and n_y to random numbers between -0.25 and +0.25 then using the unit length of the director to determine n_z. One can qualitatively think of this noise as related to thermal director fluctuations. We have found that the amplitude of this random noise does not affect the director dynamics in any significant way.

We followed the report of Fedak et al [9] to estimate the elastic constants in our system to include the effect of the large percentage (40%) of chiral additive (CB15 from Merck) in the system on the elastic constants. These

authors experimentally measured the elastic constants of a mixture as a function of weight percentage when both enantiomers of CB15 were added to a nematic host. The authors found a reduction of 61.5%, 58.8%, and 48.6% for K_{11}, K_{22} and K_{33} respectively. We can include this effect by reducing the elastic constants of our system by these same percentages. We used MLC 6080 from Merck as the nematic host for this study. We chose this material for its large birefringence ($\Delta n = .2024$) and low viscosity ($\gamma_1 \approx 0.133$). The values of the elastic constants for our system were thus adjusted from 14.4, 7.1, and 19.1 pN to 8.86, 4.17 and 9.28 pN for K_{11}, K_{22} and K_{33} respectively.

To our knowledge, no work has been done investigating the effect of chiral concentration on the rotational viscosity. However, the rotational viscosity is only used to scale time in simulations, therefore we may rescale time to coincide with the data. Similarly, no work has been done to the authors' knowledge of the effects of the chiral additive on the dielectric constants or refractive indices. The dielectric constants can be determined experimentally from capacitance measurements. To determine $\varepsilon_\perp$, we let the planar cell relax into the perfect planar state over a period of a few days. Then we measured the capacitance using 0.1 V as the probing voltage. From this we measured $\varepsilon_\perp$ to be $5.51 \pm .05$. To measure $\varepsilon_\parallel$, we applied a high probing voltage (50V) to the homeotropic sample and measured the capacitance. This yielded a value of 14.31 ± 0.5 for $\varepsilon_\parallel$. To determine the indices of refraction, we used a weighted average of the host and the chiral values. The refractive indices have never been measured for CB15, however the chemical structure of CB15 is very similar to the nematic 5CB, with the exception that CB15 has a chiral center in the alkyl chain [10]. Therefore, the values for 5CB were used when calculating the average [11]. The indices of refraction for the nematic host are 1.7100 and 1.5076 for the extraordinary and ordinary indices of refraction. For 5CB, these values are 1.7212 and 1.5376, yielding weighted averages of 1.7145 and 1.5196.

For the purposes of this study, we assumed the scalar order parameter, S, to be constant in space. This simplification does not allow for introduction of defects having an isotropic core. This assumption implies that the system transforms from the **H** state to the **FC** state in a continuous manner. The validity of this assumption was tested by comparing the free energy density at every lattice point with the free energy density of a defect core. This assumes that the free energy density is constant between grid points. This simplification can only introduce a small error due to the fact that the grid spacing is not much larger than a molecular length. The grid spacing for these calculations was 25.4 nm per grid point, and molecular lengths for standard nematic liquid crystals are on the order of 10 nm [1]. Because our grid spacing is roughly the same as a molecular length, the free energy of a defect core can be estimated to be on the order of $K \times l_0$, where K is an average elastic constant and l_0 is a molecular length [1]. This core has a

length scale on the order of a molecular length [1]. Therefore, the free energy density of a defect core should be roughly K / l_0^2. For our system, this free energy density evaluates to roughly 75,800 Jm^{-3}. We found the free energy density to always be at least a factor of 50 times smaller than that required for isotropic regions to form, with the highest values occurring at the homeotropic boundaries. Two such calculations showing this free energy density and director configurations are shown in figure 1. Figure 1 (a) shows a typical energy density diagram for the calculation with rubbed planar boundaries and figure 1 (b) shows a typical energy density diagram for the calculation with homeotropic boundary conditions. We can therefore say that introduction of regions containing isotropic cores acts to increase the free energy of the system, thus excluding them from consideration.

The director configurations during the transition from the **H** state to the **FC** state are shown in figures 2 and 3. Figure 2 shows the transition for the sample with rubbed planar boundary conditions, while figure 3 shows the director configuration as a function of time for the homeotropic boundary condition sample. These figures are down-sampled from a 197 x 197 computational grid. The thicknesses in the x and z-directions were 5.0 μm.

For this simulation, we used periodic boundary conditions in the x and y directions. During the initial stages of the transition, the system transforms through a 1-dimensional relaxation. Thus, during this part of the transition, the periodic boundary conditions have no effect. The preliminary results for the transition from the **TP** state to the **FC** state show feature sizes much smaller than 5 μm, thus indicating that the periodic boundary conditions again have little or no effect. We have performed this calculation for other values of thickness to pitch ratio, and found very little dependence, also suggesting the periodic boundary conditions have little or no effect.

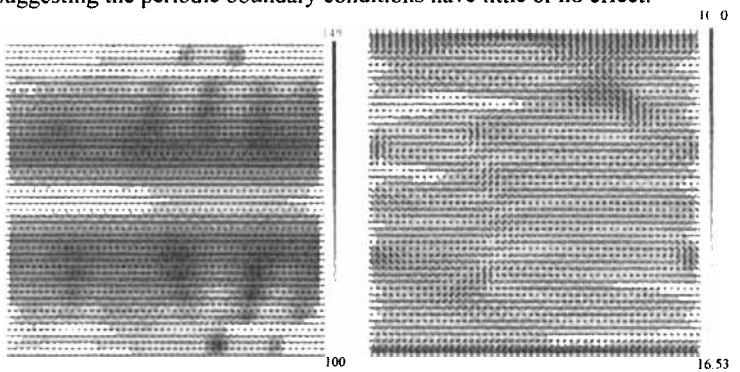

(a) (b)

Figure 1. Example free energy density calculations for the (a) planar sample and (b) homeotropic sample. The units on the scales are J m^{-3}.

EXPERIMENTAL

To verify the accuracy of the simulation, we prepared two samples, one with strong planar anchoring at the boundaries and the other with strong perpendicular (homeotropic) anchoring at the boundaries. The planar boundary conditions were achieved by spin coating an organic polyimide (Dupont 2555) which was then rubbed with a felt cloth. The pretilt angle in a sample filled with the nematic host was measured by the magnetic null method to be (3.75 ± 0.5) degrees. The homeotropic boundary conditions were achieved by spin coating a strong homeotropic surfactant (Aldrich Octadecyltrichlorosilane, which we will refer to as "silane"). By mixing 40% by weight of chiral (CB15 from Merck) with a nematic host (MLC 6080 from Merck) we were able to obtain a reflection in the visible region.

The method used to measure the pitch of the material uses the relation between the reflected spectrum and the pitch, $\lambda_{max} = \langle n \rangle \times P_0$. From the average indices of refraction given above, we obtain an $\langle n \rangle$ for the mixture of 1.6170. If the planar sample is allowed to relax into the **P** state for a few hours, the 'perfect' **P** state appears. This state has nearly all reflecting helices aligned perpendicular to the substrates [12]. By measuring the reflectance spectrum for the 'perfect' **P** state in the planar sample, the wavelength of peak reflectance was found to be (580 ± 10) nm. This yields a P_0 of (358.7 ± 6.2) nm. The sample thicknesses were controlled by 5 μm glass cylinders and were measured by interference methods to be (5.0 ± 0.2) μm for both samples. This gives a thickness to pitch ratio (d/P_0) of 13.9 ± 0.6. This value was used in the simulations.

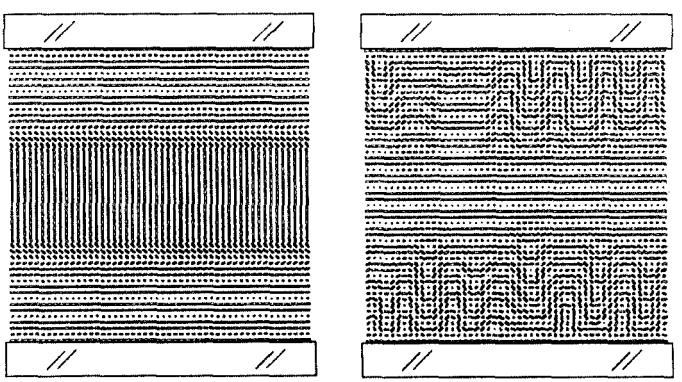

Figure 2. Simulated director configuration during the transition from the homeotropic state to the focal conic state for the planar sample. Times are: (a) 1.1 ms and (b) 3 ms. Substrates are shown for clarity.

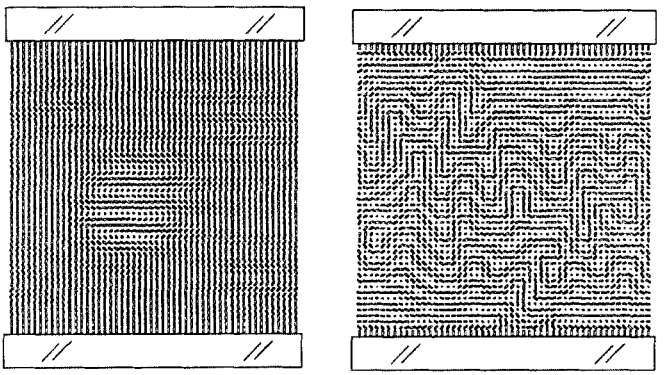

(a) (b)

Figure 3. Simulated director configuration during the transition from the homeotropic state to the focal conic state for the homeotropic sample. Times are: (a) 0.91 ms and (b) 3 ms.

The critical voltage to obtain the **H** state can be calculated by multiplying equation (1) by the sample thickness. For our system, this critical voltage was approximately 30 Volts. In the experiments performed here, the voltage applied to obtain the **H** state was always greater than or equal to 50 volts. To allow the system to transform to the **FC** state, it is necessary to drop the voltage from the **H** state value not to zero, but to an intermediate bias voltage. Equation (2) can be used to determine the correct value of the bias. For our system, this yields a voltage of roughly 13 V, agreeing well with our experimental values of 15 volts for the rubbed planar sample and 10 volts for the homeotropic sample. These values were also used in calculations.

Two experiments were performed to verify the numerical simulations. First, we measured the capacitance of the samples as a function of time. This can be accomplished by connecting a known capacitance, C_0, in series with the sample and measuring the voltage across the known capacitance as a function of time [13]. The equation for the capacitance of the sample is derived in equation (6). To ensure the voltage drop across the liquid crystal sample was very close to the applied voltage, we set $C_0 >> C_{LC}$. In our experiment, the value of C_0 was 0.455μF, and the driving frequencies were 4kHz and 10kHz for the planar sample and the homeotropic sample respectively. These frequencies were low enough to allow full charging.

$$\frac{V_{measured}}{V_{applied}} = \frac{C_{total}}{C_0}, \quad \frac{1}{C_{total}} = \frac{1}{C_0} + \frac{1}{C_{LC}}, \quad C_{total} = \frac{C_0 C_{LC}}{C_0 + C_{LC}} \cong C_{LC}, \Rightarrow C_{LC} \cong C_0 \frac{V_{measured}}{V_{applied}} \quad (6)$$

The capacitance of a dielectric sample between two conducting plates is given by equation (7).

$$C = \varepsilon \varepsilon_0 A / d_Z \quad (7)$$

Where ε is the relative permittivity or dielectric constant, ε_0 is the permittivity of free space (= 8.85×10^{-12} Fm^{-1} in MKS units), A is the area of the plates, and d_Z is the spacing between the plates, in this case the sample thickness. However, the dielectric constant of a liquid crystal system is anisotropic, and therefore depends on director orientation. Hence an average dielectric constant, given in equation (8), must be used.

$$\bar{\varepsilon} = \frac{1}{N_X}\sum_X \frac{1}{\frac{1}{N_Z}\sum_Z \frac{1}{\varepsilon_i}} \quad \text{,where } \varepsilon_i = \varepsilon_{\parallel}\cos^2\theta_i + \varepsilon_{\perp}\sin^2\theta_i \tag{8}$$

Here N_X is the number of lattice points in the x-direction, N_Z is the number of lattice points in the z-direction, and θ is the angle between the director and the z-axis.

For the planar sample, the X-Z plane is different from the Y-Z plane because of the directional nature of the boundary conditions induced by the rubbing. To take this into account, the simulations were performed in both planes and the effective dielectric constant was averaged. The calculated director configurations had no significant differences, probably due to the fact that the d/P_0 ratio is quite large.

The rotational viscosity for the simulation must be adjusted to take into account the high percentage of chiral. It was found that a good fit was obtained if the rotational viscosity (which scales time) was reduced by a factor of 3.3. This shift can be explained by the fact that adding a large amount of CB15 (which is isotropic at room temperature) lowers the transition temperature [14], thereby reducing the viscosity. The rotational viscosity drops by approximately a factor of 2 every 10 degrees C [14]. This suggests that the transition temperature dropped by about 17 degrees C. Therefore, we renormalized time for the simulation using: $t_{new} = t_{old} / 3.3$.

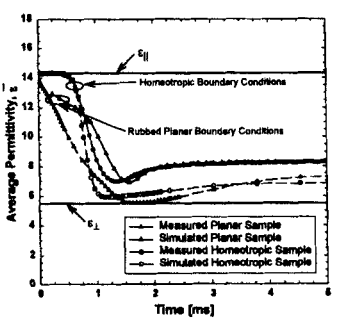

Figure 4. Dynamics of the effective dielectric constant. The solid lines and symbols represent the experimental results and the dashed lines and open symbols represent the simulation results.

The average dielectric constant as a function of time for the two samples is shown in figure 4. The reader will note that the average dielectric constant for homeotropic boundary conditions is held for a short time in the **H** state, while the planar sample starts relaxing immediately. The curves for both boundary conditions reach a minimum slightly after 1 ms. The fact that, at this minimum, the value of the average dielectric constant is close to the value of $\varepsilon_{\perp}$ implies a director configuration where the average polar angle of the director is close to 90 degrees. This condition is satisfied by the **TP** state. However, the experimental results do not show the **TP** state being as "perfect". This could be caused by any combination of factors. The Helfrich-like distortions do not occur in the model unless there is noise. If noise were added differently, this could influence the **TP** state. Also, the given values of the elastic constants when CB15 is mixed at 40% with MLC 6080 are only approximate. A shift in the K_{33}/K_{22} ratio could also affect this state. Finally, the fact that the simulation is restricted to 2 spatial dimensions might also play a role.

For the second experiment, we connected an Oriel flash lamp to a Nikon Optiphot-2 polarizing microscope. The flash lamp is triggered by a delay box, which delays the trigger from a Stanford Research Model DS345 Function Generator. The measured duration of the flash is approximately 9 ns. This ensures that we get clear pictures at precisely the time we desire. For the homeotropic sample, no domains existed at 0.75 ms, however domains could be seen at 1.0 ms. This implies that domain formation began at 0.825 ± 0.125 ms. A similar analysis for the planar sample gives domain formation starting at 1.125 ± 0.125 ms. The simulations show the onset of a periodic structure that eventually leads to domains starting at approximately the same times.

DISCUSSION AND CONCLUSIONS

The numerical simulations show the director configuration transforming to the **TP** state on the way from the **H** state to the **FC** state for the values of applied voltage used here for both planar and homeotropic boundary conditions. This transition to the **TP** state is accomplished via a one-dimensional relaxation. It has been theoretically suggested that the pitch of the **TP** state should be $K_{33}/K_{22} \times P_0$ [4]. For our system, this quantity evaluates to (800.2 ± 13.8) nm. The pitch of the **TP** state found in experiment is (609.2 ± 6.2) nm for the planar sample, suggesting that the pitch winds up somewhat during this conical relaxation. The pitch is more difficult to measure in the homeotropic sample because the reflectance peak is broad, but can be estimated to be (563.3 ± 62.0) nm. The simulations give the pitch in the bulk to be (612.2 ± 12.7) nm for the planar sample and (714.3 ± 62.0) nm for the homeotropic sample. The large uncertainty for the homeotropic sample is due to the distribution of pitches in the sample. The discrepancy in

the homeotropic data could be caused by errors in the elastic constants used in simulation. This is not a problem for the planar sample, where the boundary conditions force the system into an integer number of turns.

The simulations suggest that the **TP** state grows in from the surfaces for planar boundary conditions and from the bulk for homeotropic boundary conditions. This agrees with Mi et al. who performed a 1-D simulation of the transition from the **H** state to the **P** state [15].

Our preliminary calculations for the latter part of the transition suggest that the **TP** state transforms to the **FC** state through a Helfrich-like undulation distortion [16], not through the introduction of isotropic regions. This is very similar to what we have recently found for the transformation process from the **TP** state to the **P** state [17]. This distortion during the transition from the **TP** state to the **FC** state grows from the surface in the planar sample while in the homeotropic sample, it grows from the bulk (see figures 2 and 3).

ACKNOWLEDGEMENTS

This work was partially funded by NSF ALCOM grant DMR 89-20147

References

[1] P.G. de Gennes and J. Prost, *The Physics of Liquid Crystals*, (New York: Oxford University Press) (1993).

[2] D. Davis, A. Kahn, X.Y. Huang, J.W. Doane, SID Dig. Tech. Pap., **29**, 901 (1998).

[3] W. Greubel, Appl. Phys. Lett., **25**, 5 (1974).

[4] D.-K. Yang, Z.-J. Lu, SID 95 Dig. Tech. Pap., 351 (1995).

[5] J.E. Anderson, P. Watson, P.J. Bos, SID Dig. Tech Pap, **30**, 198–201 (1999).

[6] D.W. Berreman, Appl. Phys. Lett., **25**, 12–15 (1974).

[7] S. Dickmann, J. Eschler, O. Cossalter, D.A. Mlynski, SID Dig. Tech. Pap., 638 (1993).

[8] Hiroyuki Mori, Eugene C. Gartland, Jr., Jack R. Kelly, Philip J. Bos, Jpn. J. Appl. Phys., **38**, 135–146 (1999).

[9] I. Fedak, R.D. Pringle and G.H. Curtis, M.C.L.C., **82**, 173 (1982).

[10] Information supplied by Merck.

[11] L.M. Blinov, V.G. Chigrinov, *Electrooptical Effects in Liquid Crystal Materials*, (New York: Springer-Verlag) (1994).

[12] P. Watson, V. Sergan, J.E. Anderson, J. Ruth, P.J. Bos, Liquid Crystals, **26**, 731–736 (1999).

[13] X.-Y. Huang, Doctoral Thesis, Kent State University (1996).

[14] W.H. deJeu, *Physical Properties of Liquid Crystalline Materials*, (New York: Gordon and Breach Science Publishers) (1980).

[15] Xiang-Dong Mi and Deng-Ke Yang, SID 98 Dig. Tech. Pap., 909 (1998).

[16] W. Helfrich, Appl. Phys. Lett., **17**, 531 (1970).

[17] P. Watson, J.E. Anderson, V, Sergan, P.J. Bos, Liquid Crystals, **26**, 1307–1314 (1999).